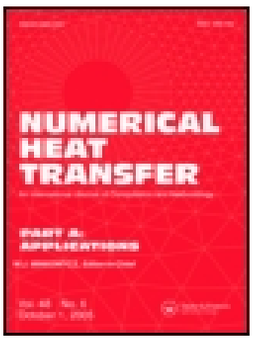

Numerical Heat Transfer, Part A: Applications

ISSN: 1040-7782 (Print) 1521-0634 (Online) Journal homepage: https://www.tandfonline.com/loi/unht20

NUMERICAL SIMULATION OF TWO-DIMENSIONAL MELTING AND RESOLIDIFICATION OF A TWO-COMPONENT METAL POWDER LAYER IN SELECTIVE LASER SINTERING PROCESS

Tiebing Chen & Yuwen Zhang

To cite this article: Tiebing Chen & Yuwen Zhang (2004) NUMERICAL SIMULATION OF TWO-DIMENSIONAL MELTING AND RESOLIDIFICATION OF A TWO-COMPONENT METAL POWDER LAYER IN SELECTIVE LASER SINTERING PROCESS, Numerical Heat Transfer, Part A: Applications, 46:7, 633-649, DOI: 10.1080/104077890504177

To link to this article: https://doi.org/10.1080/104077890504177

Published online: 17 Aug 2010.

Numerical Heat Transfer, Part A, 46: 633–649, 2004

ISSN: 1040-7782 print/1521-0634 online
DOI: 10.1080/104077890504177

Taylor & Francis
Taylor & Francis Group

NUMERICAL SIMULATION OF TWO-DIMENSIONAL MELTING AND RESOLIDIFICATION OF A TWO-COMPONENT METAL POWDER LAYER IN SELECTIVE LASER SINTERING PROCESS

Tiebing Chen and Yuwen Zhang
Department of Mechanical and Aerospace Engineering, University of Missouri—Columbia, Columbia, Missouri, USA

Selective laser sintering (SLS) of metal powder is an emerging technology by which metal parts can be fabricated in a layer by layer fashion. SLS of the first layer is modeled as melting and resolidification of a metal powder layer subject to a moving heat source on top, while the bottom is adiabatic. SLS of the consecutive layer is modeled as melting and resolidification of a metal powder layer on top of the existing multiple resolidified layers. The results indicate that the thicknesses of the loose metal powder layer, the moving heat source intensity, and the scanning velocity have significant effects on the sintering process in both the first layer and each subsequent layer. A parametric study is performed, and the best combination of processing parameters is recommended.

1. INTRODUCTION

Solid freeform fabrication (SFF) is an emerging technology in the rapid prototyping field. Direct selective laser sintering (SLS) of metal powders is a desirable SFF process by which functional and fully dense metal parts can be manufactured layer by layer from computer-aided design (CAD) data in a short time period and relatively few number of stages [1]. High-power continuous-wave CO_2 lasers and near-infrared pulsed Nd:YAG lasers are both commonly used in direct SLS processes. In most applications, a CO_2 laser is used so that the powder is nearly homogeneously heated and sintered.

The direct SLS process is complex; therefore, the specific metal powders used must be chosen carefully. One problem in the metal powder sintering process is the "balling" phenomenon, which is the formation of a series of spheres with the approximate diameter of the laser beam. The tensile force on the surface of the molten metal is not enough to force the metal liquid into a horizontal layer-wise geometry, because the molten metal is contained entirely by loose powders rather than fully

Received 7 November 2003; accepted 12 May 2004.
Support for this work by the U.S. Office of Naval Research under Grant N00014-02-1-0356 is gratefully acknowledged.
Address correspondence to Yuwen Zhang, Department of Mechanical and Aerospace Engineering, University of Missouri—Columbia, E3411 Engineering Building East, Columbia, MO 65211, USA. E-mail: zhangyu@missouri.edu

NOMENCLATURE

b	moving heat source half-width, m	x	moving horizontal coordinate, m
Bi	Biot number ($=hb/k_H$)	X	dimensionless moving horizontal coordinate ($=x/b$)
c_p	specific heat, J/kg K		
C	dimensionless heat capacity ($=C^0/C_H^0$)	z	vertical coordinate, m
C^0	heat capacity ($=\rho c_p$), J/m^3 K	Z	dimensionless vertical coordinate ($=z/b$)
h	convective heat transfer coefficient, W/m^2 K	α	thermal diffusivity, m^2/s
h_m	latent heat of melting or solidification, J/kg	α_a	absorbtivity
		δ	powder-layer thickness, m
I_0	heat source intensity at the center of the heat source, W/m^2	δ	dimensionless powder-layer thickness ($=\delta/b$)
k	thermal conductivity, W/m K	ΔT	one-half of dimensionless phase-change temperature range
K	dimensionless thermal conductivity ($=k/k_H$)	ΔT^0	one-half of phase-change temperature range, K
N	numbers of sintered layers under the loose powder layer	ε	volume fraction of gas (porosity for unsintered powder) $[=V_g/(V_g+V_L+V_H)]$
N_i	dimensionless moving heat source intensity $[=\alpha_a I_0 b/k_H(T_m^0-T_i^0)]$	ε_e	emissivity of surface
		η	dimensionless solid–liquid interface location ($=s/b$)
N_R	Radiation number $[=\varepsilon_e\sigma(T_m^0-T_i^0)^3 b/k_H]$	η_{st}	dimensionless sintered depth ($=s_{st}/b$)
N_t	temperature ratio for radiation $[=T_m^0/(T_m^0-T_i^0)]$	η_0	dimensionless location of the surface ($=s_0/b$)
s	solid–liquid interface location, m	ρ	density, kg/m^3
s_0	location of surface, m	σ	Stefan-Boltzmann constant, ($=5.67\times10^{-8}$ W/m^2 K^4)
s_{st}	sintered depth, m	τ	dimensionless false time ($=\alpha_H t/b^2$)
Sc	subcooling parameter $[=C_H^0(T_m^0-T_i^0)/(\rho_L h_m)]$	ϕ	volume percentage of low-melting-point powder $[=V_L/(V_L+V_H)]$
t	false transient time, s		
T	dimensionless temperature $[=(T^0-T_m^0)/(T_m^0-T_i^0)]$	**Subscripts**	
T^0	temperature, K		
u	heat source moving velocity, m/s	eff	effective
U	dimensionless heat source moving velocity ($=ub/\alpha_H$)	H	high-melting-point powder
		L	low-melting-point powder
V	volume, m^3	m	melting point
w	velocity of liquid phase, m/s	p	sintered parts
W	dimensionless velocity of liquid phase ($=wb/\alpha_H$)	s	solid

dense material. Another problem lies in achieving dimensional stability during the sintering process. This results from shrinkage, causing poor bonding between the scanning lines and layers. Two different metal powder systems have been developed in order to solve the problems mentioned above. One is the single-component powder approach, which overcomes the "balling" phenomenon by scanning at very high velocities with very small beam spot sizes [2], and the other is the two-component powder approach, which uses two types of the metal powders possessing significantly different melting points [3, 4]. The high-melting-point powder remains solid in the sintering process and plays an important role as the support structure necessary to avoid "balling." Solidification of the low-melting-point metal bonds the high-melting-point metal powder particles together to form the part layers. The particular material

properties and methods of material analysis of the metal-based powder system for SLS applications are addressed by Storch et al. [5]. Effects of laser sintering processing parameters on the microstructure and densification of iron powder were investigated by Simchi and Pohl [6]. A case study on the development of direct metal laser sintering for rapid tooling was performed by Simchi et al. [7]. A thorough examination of direct SLS in addition to fundamental issues in SFF was addressed by Lu et al. [8].

Melting and resolidification are the mechanisms that bond powder particles together to form a part layer, and they are also the mechanisms that bond different layers together to form a functional part. Fundamentals of melting and solidification have been investigated extensively, and detailed reviews are available in the literature [9, 10]. The distinctive feature of melting in SLS of a two-component metal powder is the significant density change due to shrinkage, which was demonstrated experimentally by Zhang et al. [11] and by Buckley and Bergman [12]. The powder layer collapses upon melting of low-melting-point metal powder particles, since the high-melting-point metal powder alone cannot sustain the powder-layer structure. The liquid–solid phase change during melting of a two-component packed bed was investigated by Mughal and Plumb numerically [13], and a constant-porosity model was developed. A one-dimensional melting problem in a semi-infinite powder bed containing a two-component powder mixture subjected to constant heat flux heating was solved analytically by Zhang and Faghri [14]. An analytical solution of one-dimensional melting of the two-component metal powder layer with finite thickness was obtained by Chen and Zhang [15]. A two-dimensional transient model of the laser melting problem with a moving laser beam, in which the interface energy balance was neglected, was developed by Chan et al. [16]. A two-dimensional steady-state laser melting problem using an alternative direction implicit (ADI) scheme with a false transient formulation was solved by Basu and Srinivasan [17]. Melting and resolidification of a subcooled semi-infinite two-component metal powder bed with a moving Gaussian laser beam was simulated by Zhang and Faghri [18], which is an approximation of SLS for the first layer of metal powder.

SLS is a process by which a functional part is fabricated by sintering metal powder layers together layer by layer, with the exception of the first layer; each layer is fabricated by sintering a loose powder layer on top of an existing sintered layer. The effects of the dominant processing parameters, such as moving laser beam intensity and scanning velocity on the two-dimensional sintering process in the finite loose metal powder layer, without or with existing sintered layers below, are considered in the present article. A thorough parametric study will be conducted, and an empirical correlation will be proposed.

2. PHYSICAL MODEL AND PROBLEM STATEMENT

Direct SLS of metal powder is a three-dimensional transient melting and resolidification problem, since the laser beam is moving over the powder layer and has a very small diameter compared with the dimension of powder layer. It is economical to simulate the sintering process in a two-dimensional, two-component metal powder layer before the real three-dimensional SLS is attempted. Figure 1 shows (*a*) the first layer of the SLS process and (*b*) a later layer with several previously sintered layers below. The physical domain is considered to be infinite

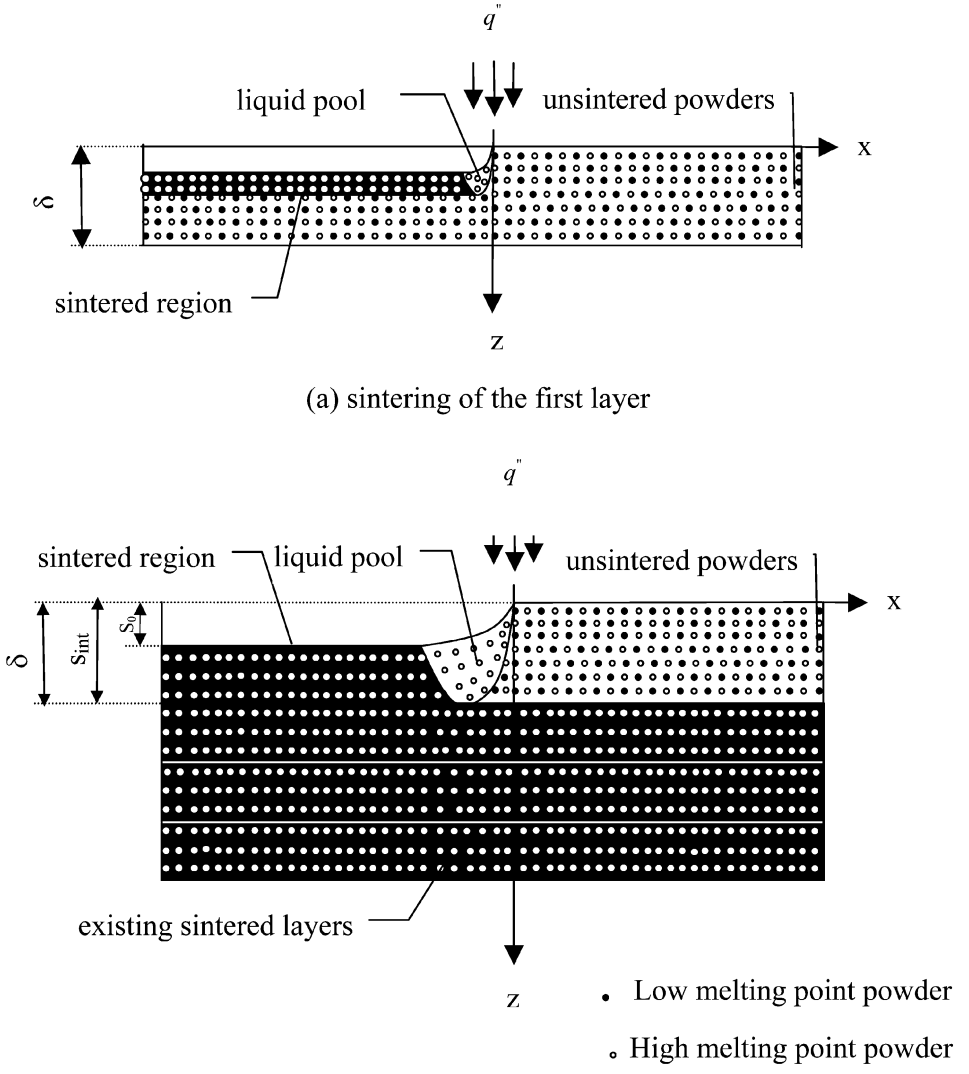

Figure 1. Physical model.

horizontally, but finite vertically. A moving Gaussian laser beam interacts with the top surface of the loose powder, and then melting is induced. In addition to having a complete understanding of the sintering process in the first layer, it is important to identify the best combination of processing parameters that allow complete sintering of the loose powders and secure bonding of the newly sintered layer to any existing sintered layers. During the simulation, the sintering depth is permitted to slightly exceed the interface of the loose powder layer and the next existing sintered layer, so that each layer can be bonded together tightly.

The following assumptions are made for the physical model.

1. Melting and resolidification in SLS is a conduction-controlled phase-change problem.
2. The thermal properties of the low-melting-point powder are the same for both liquid and solid phases.
3. Two kinds of metal powders are fully mixed, and the initial porosity is uniform.
4. The bottom of the computational domain for both cases is adiabatic.
5. The horizontal dimension of the powder layer is significantly larger than the diameter of the laser beam.

The physical model is formulated using a temperature-transforming model, which converts the enthalpy-based energy equation into a nonlinear equation, with temperature as the only dependent variable. In this methodology, the solid–liquid phase change is assumed to occur in the very small temperature range $(T_m^0 - \Delta T^0)$ to $(T_m^0 + \Delta T^0)$ [19]. The beauty of the temperature-transforming model is that a converged solution can always be obtained without limitation on grid size and time step for the conduction-controlled phase-change problem. It can also successfully model convection-controlled solid–liquid phase-change problems. A moving coordinate system, of which the origin is fixed at the center of the heat source and moved together with it at speed u, is employed. If one observes from the origin, the powder layer travels at a velocity $-u$ in the moving direction opposite the laser beam. Therefore, a convection term is introduced into the governing equation. The dimensionless governing equation for the physical problem is

$$-U\frac{\partial(CT)}{\partial X}+W\frac{\partial(CT)}{\partial Z}=\frac{\partial}{\partial X}\left(K\frac{\partial T}{\partial X}\right)+\frac{\partial}{\partial Z}\left(K\frac{\partial T}{\partial Z}\right)-\left(-U\frac{\partial S}{\partial X}+W\frac{\partial S}{\partial Z}\right) \tag{1}$$

where the dimensionless variables are defined in the Nomenclature. The dimensionless shrinkage velocity W, heat capacity C, source term S, and thermal conductivity K in Eq. (1) in the loose powder layer are different from those in previously sintered layers below. In the loose powder,

$$W=\begin{cases}-\varepsilon_s U\dfrac{\partial \eta_{st}}{\partial X} & Z\le \eta_{st}\le \Delta\\ 0 & Z>\eta_{st}\le\Delta\end{cases} \tag{2}$$

$$C=\begin{cases}(1-\varepsilon)(\phi C_L+1-\phi) & T<-\Delta T\\ (1-\varepsilon)(\phi C_L+1-\phi)+(1-\varepsilon)\phi\dfrac{C_L}{2\mathrm{Sc}\,\Delta T} & -\Delta T<T<\Delta T\\ (1-\varepsilon)(\phi C_L+1-\phi) & T>\Delta T\end{cases} \tag{3}$$

$$S = \begin{cases} 0 & T < -\Delta T \\ \dfrac{(1-\varepsilon)\phi C_L}{2\,\mathrm{Sc}} & -\Delta T < T < \Delta T \\ \dfrac{(1-\varepsilon)\phi C_L}{\mathrm{Sc}} & T > \Delta T \end{cases} \tag{4}$$

$$K = \begin{cases} K_{\mathrm{eff}} & T < -\Delta T \\ K_{\mathrm{eff}} + \dfrac{K_p - K_{\mathrm{eff}}}{2\,\Delta T}(T + \Delta T) & -\Delta T < T < \Delta T \\ K_p & T > \Delta T \end{cases} \tag{5}$$

In the resolidified region at the left side of the liquid pool and the existing sintered layers below the loose powder layer,

$$W = 0 \tag{6}$$

$$C = (1-\varepsilon)(\phi C_L + 1 - \phi) \tag{7}$$

$$S = \frac{(1-\varepsilon)\phi C_L}{\mathrm{Sc}} \tag{8}$$

$$K = K_p \tag{9}$$

where K_{eff} is the dimensionless effective thermal conductivity of the loose powder region and K_p is dimensionless thermal conductivity in the sintered region [18]. The corresponding boundary conditions of Eq. (1) are as follows:

$$-K\frac{\partial T}{\partial Z} = N_i \exp(-X^2) - N_R[(T + N_t)^4 - (T_\infty + N_t)^4] - \mathrm{Bi}(T - T_\infty) \tag{10}$$

$$Z = \eta_0(X)$$

$$\frac{\partial T}{\partial Z} = 0 \qquad -\infty \le X \le \infty \qquad Z = \Delta_s + N\Delta_p \qquad \tau > 0 \tag{11}$$

$$T = -1 \qquad |X \to \infty| \qquad 0 < Z < \Delta_s + N\Delta_p \qquad \tau > 0 \tag{12}$$

The location of the liquid surface is related to the sintered depth with the assumption that the sintered layers are fully densitified, i.e.,

$$\eta_0(X) = \varepsilon_s \eta_{st}(X) \tag{13}$$

3. NUMERICAL SOLUTION

A false transient method is employed to solve the energy equation numerically. In this methodology, a false transient term, $\partial(CT)/\partial\tau$, is included in the energy equation, and the converged steady-state solution is declared when the temperature distribution and sintering depth do not vary with the false transient time. Equation

(1) with the false transient term can be discretizied by the finite-volume method [20]. A block-off technique recommended by Patankar [20] is employed to deal with the irregular geometry of the liquid pool caused by the downward movement of the top liquid surface due to shrinkage. Therefore, the computational domain is transferred into a regular rectangle shape and the density and thermal conductivity in the empty space created by the shrinkage are set to zero. The power-law scheme [20] is used to discretize the convection-diffusion terms. A very small dimensionless phase-change temperature range, $\Delta T = 0.001$, is used in the simulation, in order to simulate melting and solidification occurring at a single temperature.

To simulate the sintering process in the finite loose metal powder layer without existing sintered layers below, the computation is carried out for a nonuniform grid in the X direction and a uniform grid in the Z direction. The origin of the coordinate system ($X = 0$, $Z = 0$) is located at the center of the top surface of the computational domain in the X direction. When there are existing sintered layers below, nonuniform grids are employed in both X and Z directions. The dimensionless thickness of each existing sintered layer can be determined by using the porosity and thickness of the loose powder layer, as indicated in the preceding section. The numerical solution is carried out for nonuniform grids in the X direction, in which the fine grids are distributed around the origin symmetrically. The fine grids zone in the X direction is greater than the width of the moving heat source. For the nonuniform grids in the Z direction, the fine grids are distributed uniformly in the loose powder layer, and the consecutive coarse grids in multiple sintered layers are set up in arithmetic progression. The grid number used in the present article is $122 \times (32–47)$, depending on the number of existing sintered layers below. Finer grid sizes were also used, but their results did not provide a noticeable difference from the present grid size.

In addition to simulating the sintering process in the single loose powder layer, the optimized combination of heat source intensity and scanning velocity is obtained when the sintering depth penetrates the bottom surface of the loose powder layer with existing sintered layers below. In order to trace the sintering depth, a small value of heat source intensity associated with a specific scanning velocity is assigned at first. The dimensionless false time step cannot be too large, since the convection term appears in the governing equation. The false time step used in the present article is $\Delta\tau = 0.01$ for $N \leq 10$ and $\Delta\tau = 0.001$ for $N = 50$. The value of the laser beam intensity is increased slightly if the sintering depth doses not increase from that of the previous heat source intensity. As the sintering depth approaches the bottom surface of the loose powder layer, the dimensionless false time step and the laser beam intensity are incrementally shifted to smaller values in order to obtain a more accurate solution. The computing procedure is finished when the sintering depth penetrates the bottom surface of the loose powder layer.

4. RESULTS AND DISCUSSION

Direct SLS was simulated in a loose powder layer with 0, 1, 2, 3, 5, 10, and 50 previously sintered layers below. The effects of dimensionless moving heat source intensity, dimensionless scanning velocity, and underlying number of previously sintered layers, which are dominant parameters for a two-dimensional sintering

process, is investigated numerically. The effect of the subcooling parameter on the sintering process is also investigated.

The sintering process in the first layer is investigated first. Figure 2*a* shows the effect of the dimensionless laser beam intensity on the sintering process ($\Delta = 0.25$, $N = 0$). It can be seen that the sintering depth increases significantly with increasing laser beam intensity, as well as the fact that the entire liquid pool moves slightly toward the positive X direction as the laser beam intensity increases. The liquid pool is quite large in the upper part, but rapidly slims down as the depth increases and is more regularly shaped as the laser beam intensity increases. When the sintering depth reaches the bottom surface of powder layer, the liquid pool becomes full. Figure 2*b* shows the effect of the scanning velocity on the sintering process ($\Delta = 0.25$, $N = 0$). It can be observed that the sintering depth decreases as the scanning velocity increases, due to the fact that the interaction between the moving heat source and the powder layer is decreased when the heat source is moved faster. The whole liquid pool moves slightly toward the opposite direction of the heat source motion as the scanning velocity increases.

Figure 3*a* shows the effect of the dimensionless moving laser beam intensity on the sintering process ($\Delta = 0.50, N = 0$). It is apparent that the sintering depth increases with increasing laser beam intensity. The liquid pool also moves slightly toward the opposite direction of the heat source motion with increasing laser beam intensity. Compared with the case in Figure 2*a*, larger laser beam intensity is needed in order to sinter the powder layer at the same scanning velocity, since more heat is conducted into the loose powder due to the thicker powder layer. The effect of the scanning velocity on the sintering process ($\Delta = 0.50, N = 0$) is shown in Figure 3*b*. As can be seen, the sintering depth decreases when the scanning velocity increases from 0.125 to 0.15. The shape of the liquid pool is similar to that in Figure 2*b*. The effect of the dimensionless moving heat source intensity on the sintering process ($\Delta = 1.0, N = 0$) is shown in Figure 4*a*. Figure 4*b* shows the effect of the scanning velocity on the sintering process ($\Delta = 1.0, N = 0$). Similar phenomena can be found in Figures 2 and 3.

In order to obtain the best combination of processing parameters when there are multiple existing sintered layers below, the sintering process is simulated when the dimensionless thickness of the top loose metal powder layer is 0.25. Figure 5 shows the combined effects of dimensionless moving heat source intensity and scanning velocity on the sintering process when there is one sintered layer below. The optimized laser beam intensities are shown in parentheses. The sintering depth penetrates the loose powder layer slightly in order to bond the newly previously layer to the existing sintered layer. It can be seen that the shapes of the liquid pools are all similar as the scanning velocity increases. The entire liquid pool also shifts slightly toward the negative X direction as the scanning velocity increases. The increment of optimized dimensionless heat source intensity is small compared with the increase of scanning velocity from 0.075 to 0.175. It is necessary to let the sintering depth penetrate past the bottom surface of the loose powder layer slightly in order to bond the layers together.

The combined effects of dimensionless moving heat source intensity and scanning velocity on the sintering process when there are two sintered layers below are shown in Figure 6. The shape of the liquid pool at each scanning velocity is

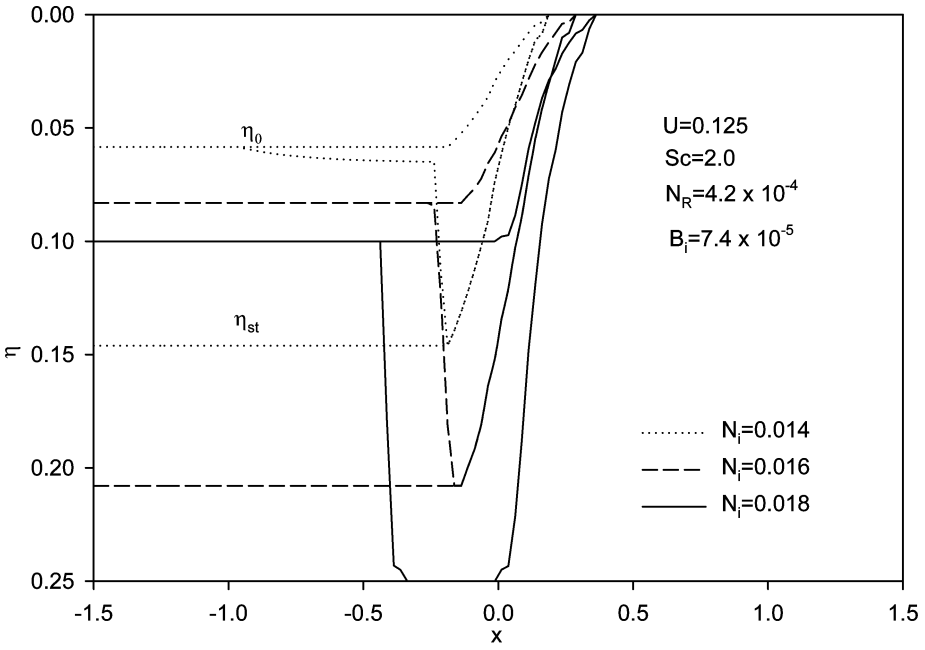

(a)

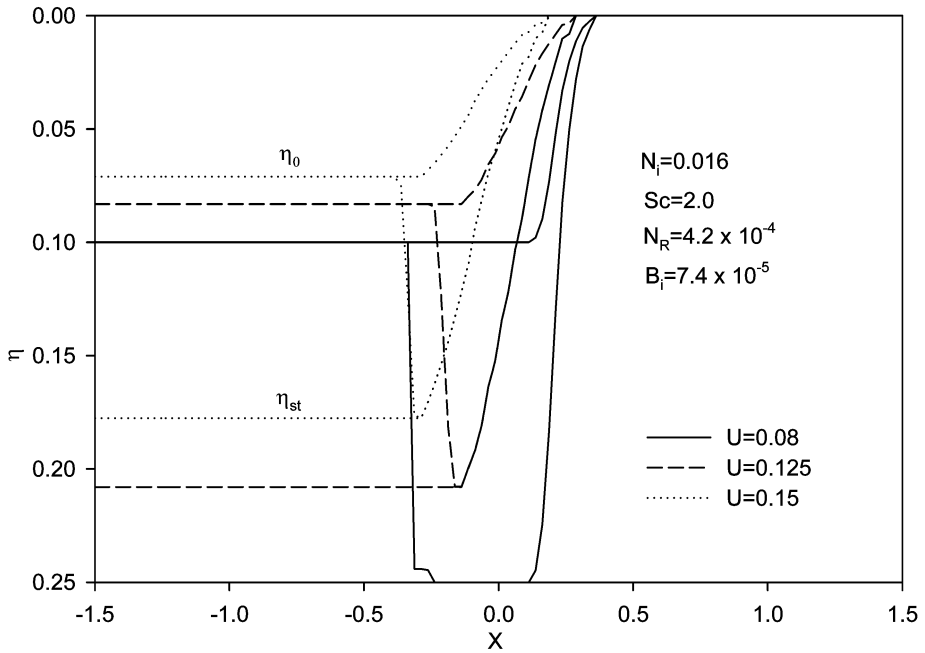

(b)

Figure 2. Effects of N_i and U on the sintering process ($\Delta = 0.25, N = 0$).

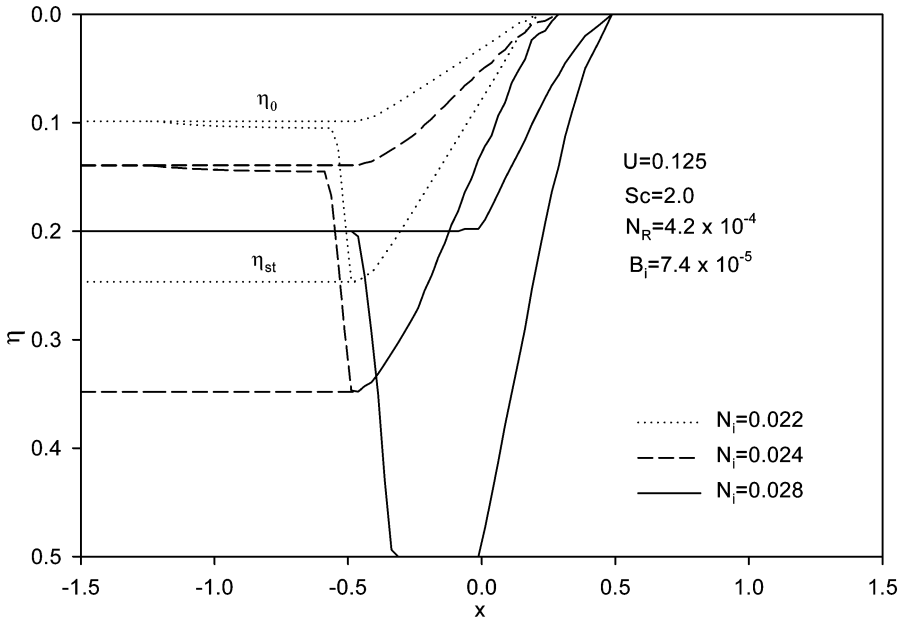

(a)

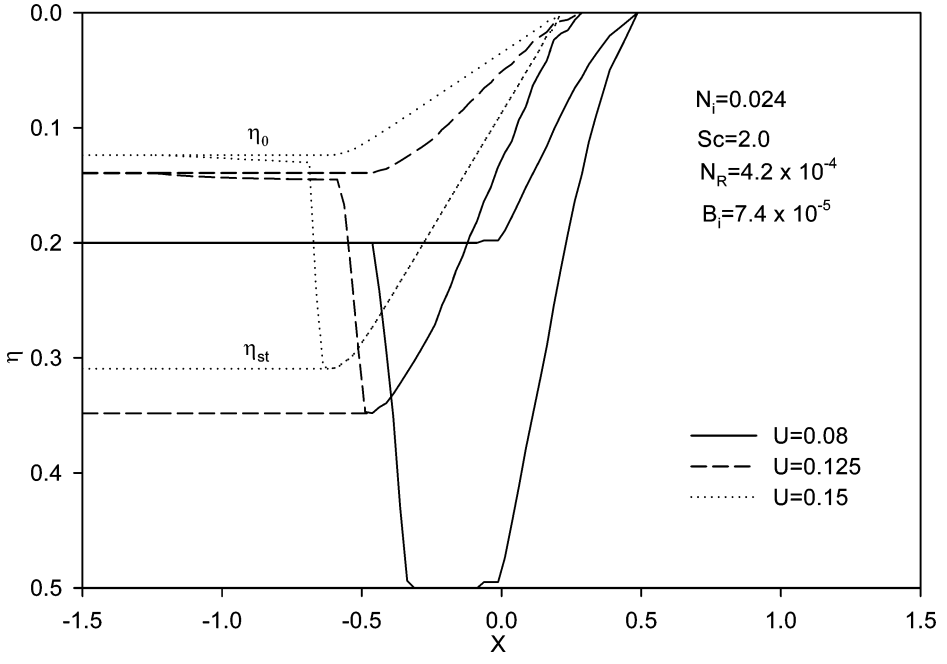

(b)

Figure 3. Effects of N_i and U on the sintering process ($\Delta = 1.0, N = 0$).

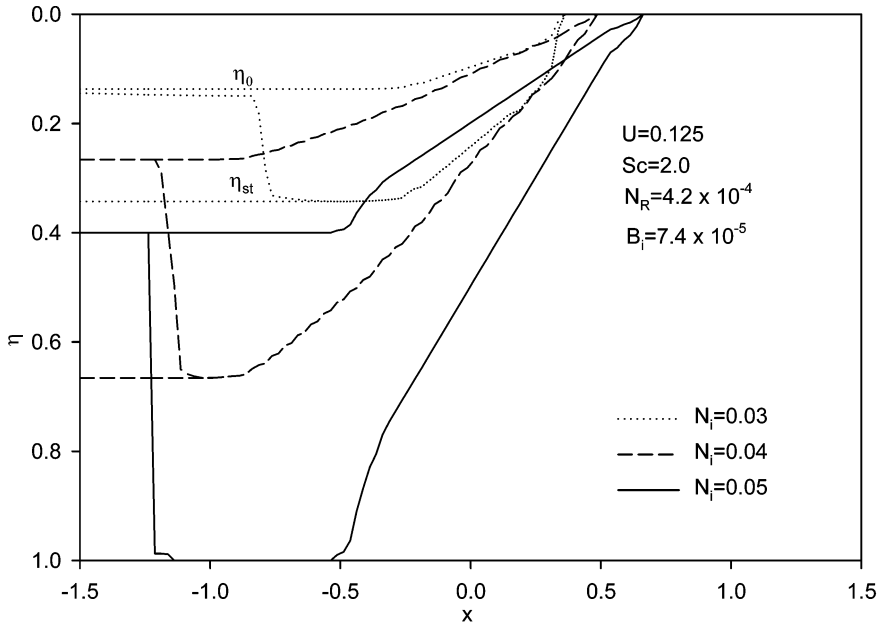

(a)

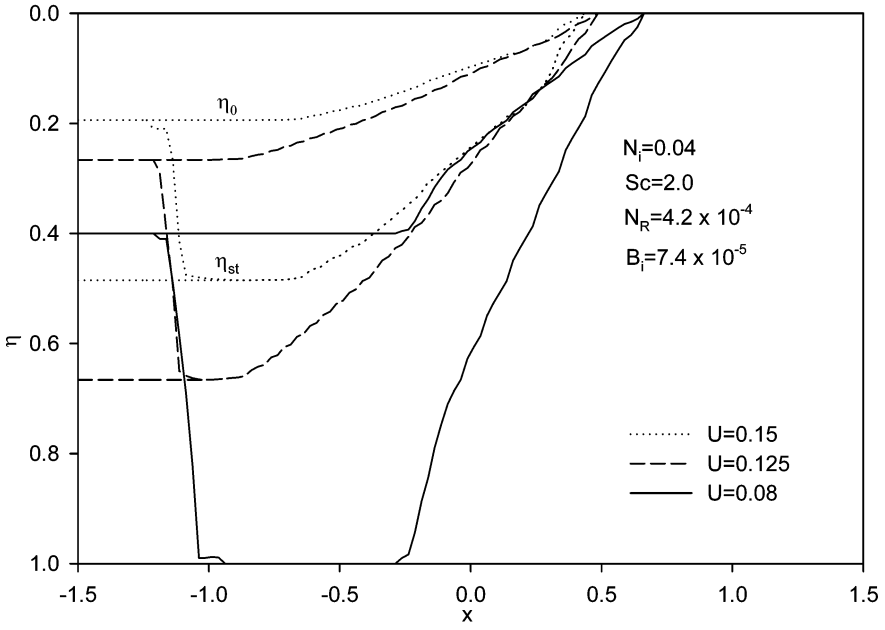

(b)

Figure 4. Effects of N_i and U on the sintering process ($\Delta = 1.0, N = 0$).

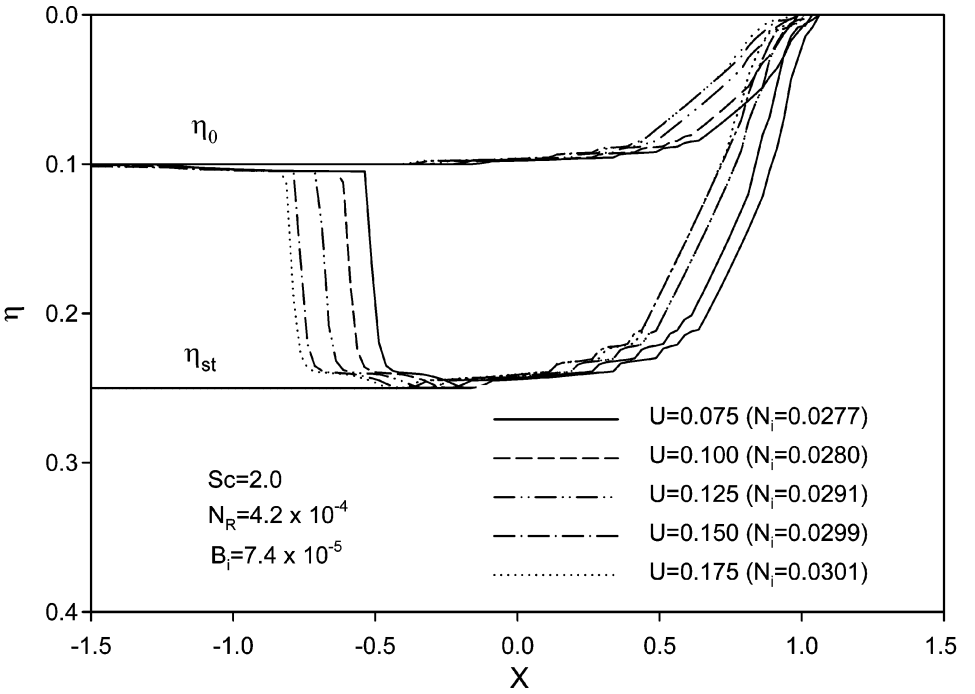

Figure 5. Combined effects of N_i and U on the sintering process ($\Delta = 0.25, N = 1$).

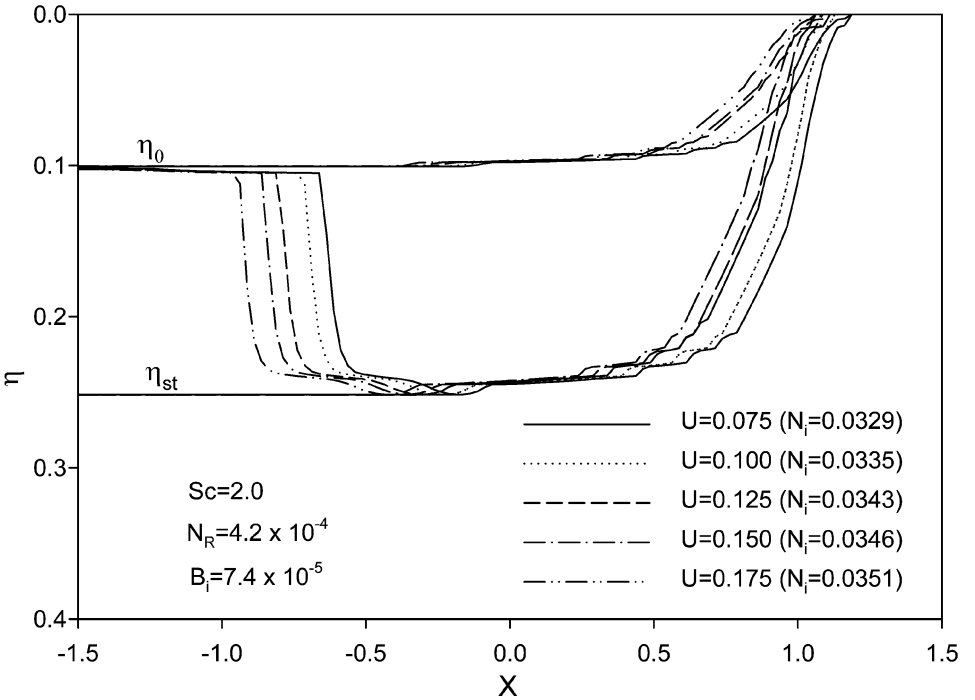

Figure 6. Combined effects of N_i and U on the sintering process ($\Delta = 0.25, N = 2$).

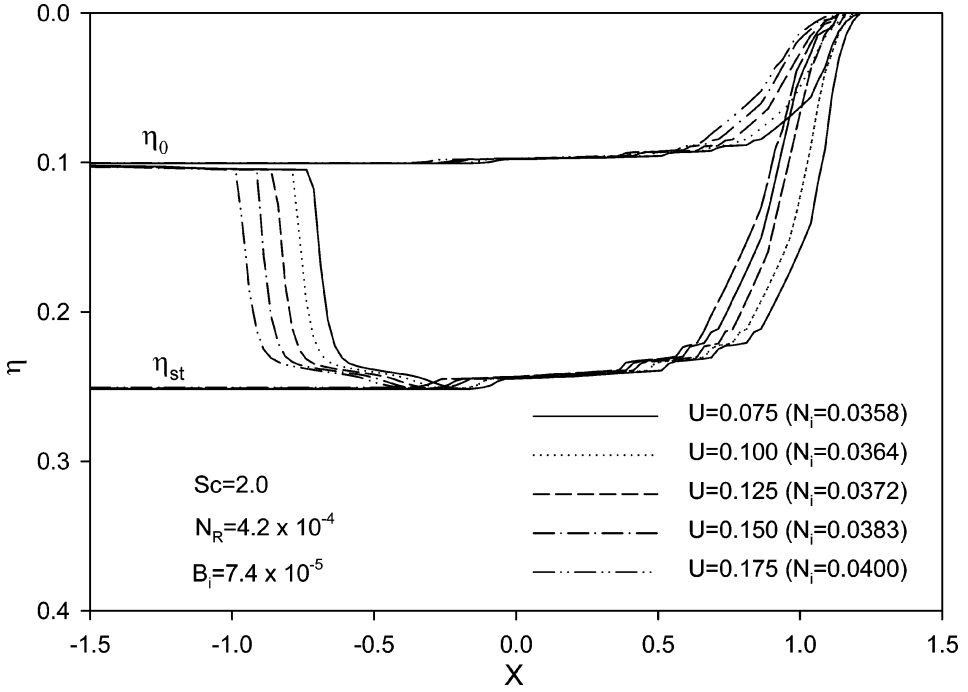

Figure 7. Combined effects of N_i and U on the sintering process ($\Delta = 0.25, N = 3$).

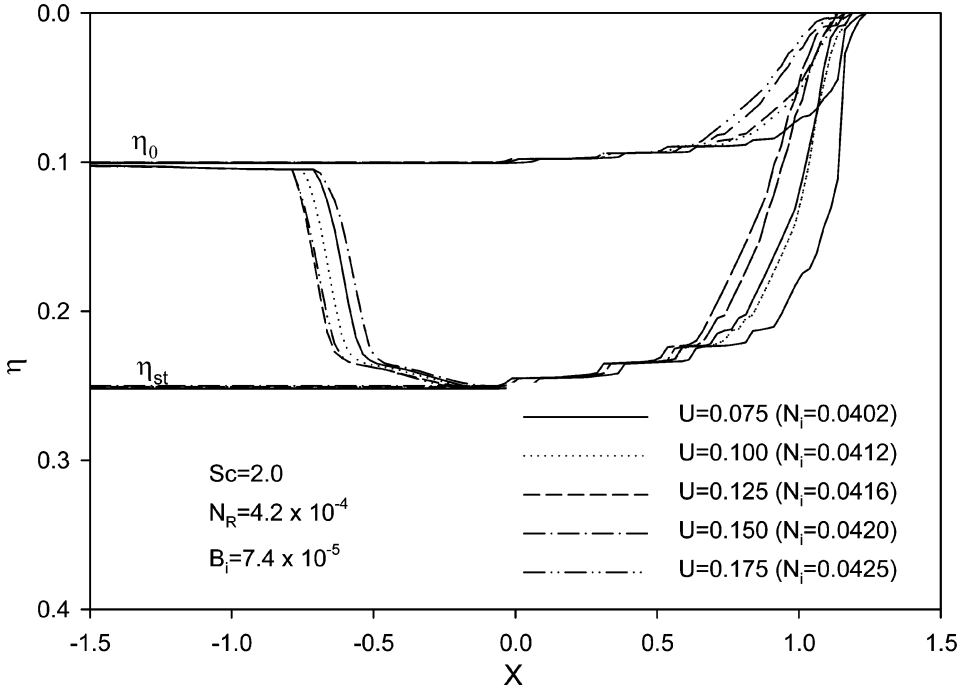

Figure 8. Combined effects of N_i and U on the sintering process ($\Delta = 0.25, N = 5$).

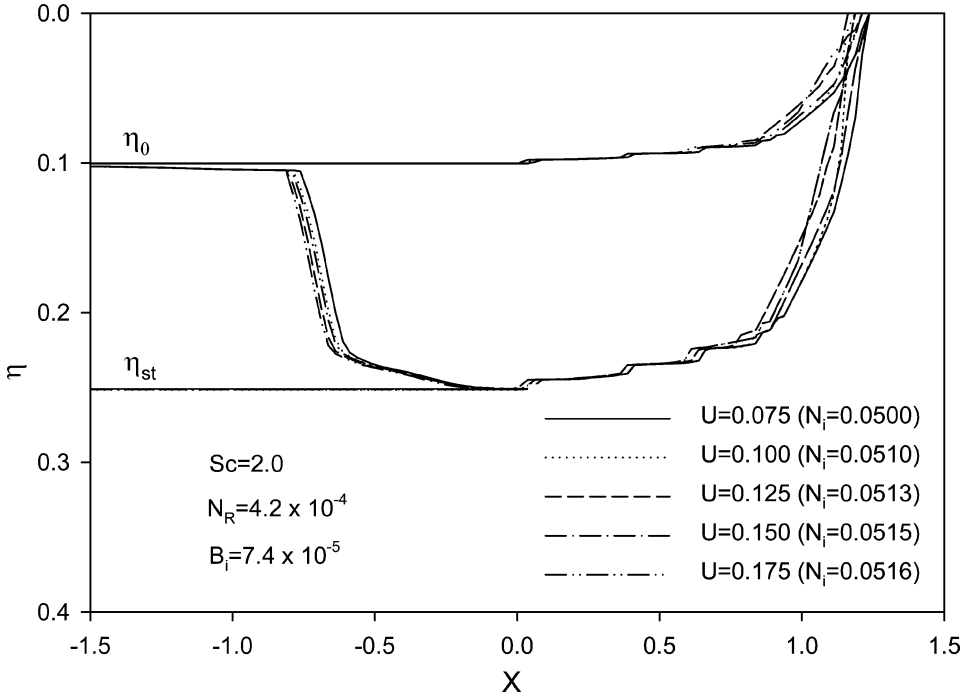

Figure 9. Combined effects of N_i and U on the sintering process ($\Delta = 0.25, N = 10$).

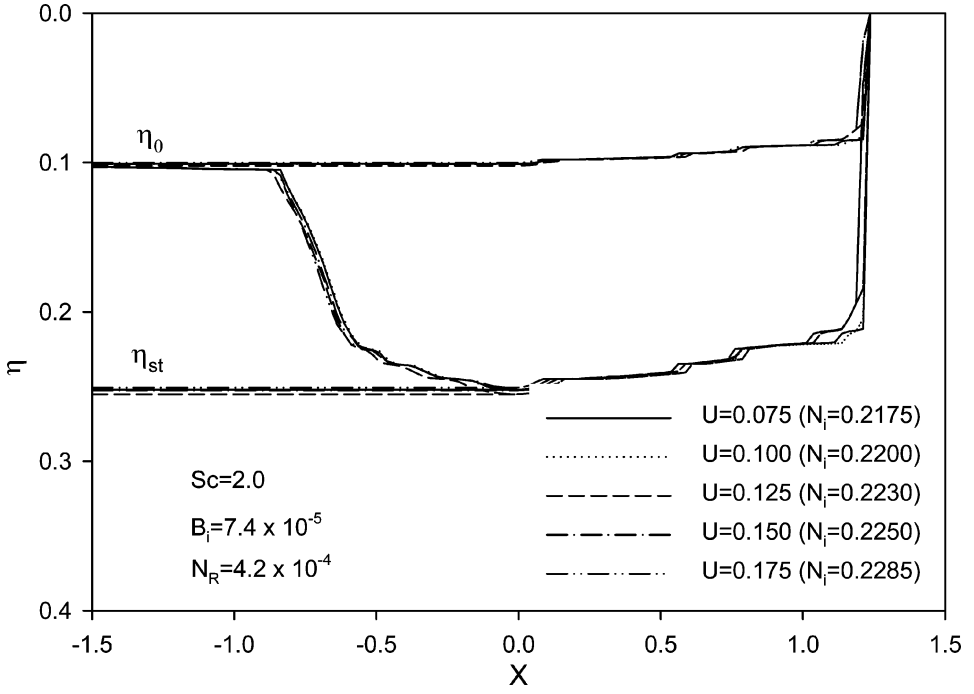

Figure 10. Combined effects of N_i and U on the sintering process ($\Delta = 0.25, N = 50$).

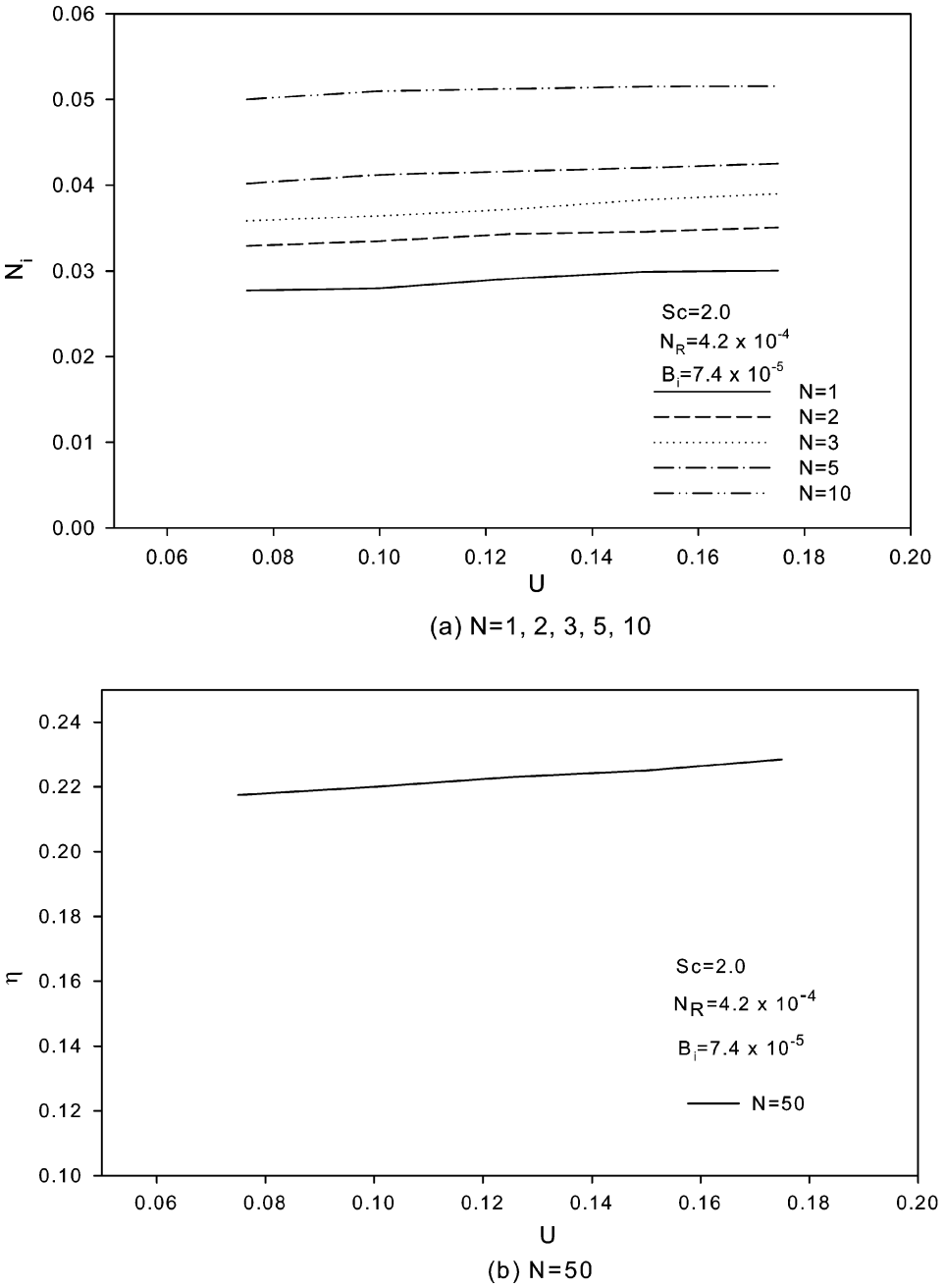

Figure 11. Optimized N_i versus U.

similar to those in Figure 5. As an extra sintered layer is added, the heat source intensity at each value of the scanning velocity increases significantly in order to obtain the same sintering depth in the loose powder layer. More heat is conducted away from the loose powder layer, since the dimensionless thermal conductivity of

Table 1. Sintering parameters applied in simulation of empirical correlation

ε_s	0.4	N_t	1.5
Sc	2.0	N_i	0.2–0.4
N_R	4.2×10^{-4}	T_∞	1.0
B_i	7.4×10^{-5}	U	0.075–0.175
Δ	0.25	ϕ	0.4
K_{LH}	2.9	C_{LH}	0.7
N	1, 2, 3, 5, 10, 50		

the sintered region is larger than that of the loose powder layer. The numerical simulations are then performed for more sintered layers below that of the loose powder, and the results are shown in Figures 7–10. Figures 7–10 show the same general trend as Figures 5 and 6, namely, that with an increasing number of underlying sintered layers, the moving heat source intensity at each scanning velocity is significantly increased. The increment of heat source intensity is similar when the added sintered layer has the same thickness. The liquid pool in the sintering process still maintains a similar shape, but its volume grows because of the larger heat source intensity needed. The fluctuation in the front side of the liquid pool also grows with an increase of sintered layers below.

In order to obtain an empirical correlation for the optimized dimensionless moving heat source intensity, a parametric study was performed, the results of which are shown in Figure 11. The parameters used in the simulation are shown in Table 1. The optimized dimensionless moving heat source intensity, N_i, is plotted as a function of scanning velocity, U, and the number of sintered layers beneath the powder layers. It can be seen that the optimized dimensionless moving heat source intensity increases with increasing scanning velocity and rises significantly when the number of underlying sintered layers is increased. The optimized dimensionless moving heat source intensity shown in Figure 11 can be correlated into the following expression:

$$N_i = A U^{-0.0045} + N^{-0.0072} \tag{14}$$

where $A = -0.9627 + 4.3930 \times 10^{-3} N$ and $U > 0$. The error of Eq. (14) is within 10%.

5. CONCLUSIONS

Melting and resolidification of a loose metal powder layer without and with multiple sintered layers underneath have been investigated numerically. The results show that the sintering depth and the shape of the liquid pool are affected significantly by the thickness of the loose powder layer, moving laser beam intensity, and scanning velocity. The optimized dimensionless moving heat source intensity increases with increasing scanning velocity in order to achieve the desired sintering depth and bond the newly sintered layer to the previously sintered layer. As the number of previously sintered layers below is increased, the optimized dimensionless moving heat source intensity at a specific scanning velocity increases significantly. An empirical correlation of the dimensionless moving heat source intensity at a specific thickness of the powder layer has been obtained.

REFERENCES

1. J. Conley and H. Marcus, Rapid Prototyping and Solid Freeform Fabrication, ASME *J. Manufact. Sci. Eng.*, vol. 119, pp. 811–816, 1997.
2. N. Karapatics, G. Egger, P. E. Gygax, and R. Glardon, Optimization of Powder Layer Density in Selective Laser Sintering, *Proc. Solid Freeform Fabrication Symp. 1999*, pp. 255–263, 1999.
3. T. Manzur, T. DeMaria, W. Chen, and C. Roychoudhuri, Potential Role of High Powder Laser Diode in Manufacturing, presented at SPIE Photonics West Conference, San Jose, CA, 1996.
4. D. Bunnell, Fundamentals of Selective Laser Sintering of Metals, Ph.D. thesis, University of Texas at Austin, Austin, TX, 1995.
5. S. Storch, D. Nellessen, G. Schaefer, and R. Reiter, Selective Laser Sintering: Qualifying Analysis of Metal Based Powder Systems for Automotive Applications, *Rapid Prototyping J.*, vol. 9, pp. 240–251, 2003.
6. A. Simchi and H. Pohl, Effects of Laser Sintering Processing Parameters on the Microstructure and Densification of Iron Powder, *Mater. Sci. Eng. A*, vol. 359, pp. 119–128, 2003.
7. A. Simchi, F. Petzoldt, and H. Pohl, On the Development of Direct Metal Laser Sintering for Rapid Tooling, *J. Mater. Process. Technol.*, vol. 141, pp. 319–328, 2003.
8. L. Lu, J. Fuh, and Y.-S. Wong, *Laser-Induced Materials and Processes for Rapid Prototyping*, Kluwer Academic, Boston, 2001.
9. R. Viskanta, Phase Change Heat Transfer, in G. A. Lane (ed.), *Solar Heat Storage: Latent Heat Materials*, CRC Press, Boca Raton, FL, 1983.
10. L. Yao and J. Prusa, Melting and Freezing, *Adv. Heat Transfer*, vol. 25, pp. 1–96, 1989.
11. Y. Zhang, A. Faghri, C. W. Buckley, and T. L. Bergman, Three-Dimensional Sintering of Two Component Metal Powders with Stationary and Moving Laser Beams, *ASME J. Heat Transfer*, vol. 122, pp. 150–158, 2000.
12. C. W. Buckley and T. L. Bergman, An Experimental Investigation of Heat Affected Zone Formation and Morphology Development during Laser Processing of Metal Powder Mixtures, *Trans. ASME*, vol. 123, pp. 586–592, 2001.
13. M. Mughal and O. A. Plumb, Thermal Densification of Metal-Ceramic Composites, *Scripta Metall. Mater.*, vol. 29, pp. 383–388, 1993.
14. Y. Zhang and A. Faghri, Melting of a Subcooled Mixed Powder Bed with Constant Heat Flux Heating, *Int. J. Heat Mass Transfer*, vol. 42, pp. 775–788, 1999.
15. T. Chen and Y. Zhang, Analysis of Melting in a Mixed Powder Bed with Finite Thickness Subjected to Constant Heat Flux Heating, *Proce. ASME Summer Heat Transfer Conf.*, Las Vegas, NV, 2003.
16. C. Chan, J. Mazumder, and M. Chen, A Two Dimensional Transient Model for Convection in Laser Melted Pool, *Metall. Trans.*, vol. 15A, pp. 2175–2184, 1984.
17. B. Basu and J. Srinivasan, Numerical Study of Steady-State Laser Melting Problem, *Int. J. Heat Mass Transfer*, vol. 31, no. 11, pp. 2331–2338, 1988.
18. Y. Zhang and A. Faghri, Melting and Resolidification of a Subcooled Mixed Powder Bed with Moving Gaussian Heat Source, *ASME J. Heat Transfer*, vol. 120, pp. 883–891, 1998.
19. Y. Cao and A. Faghri, A Numerical Analysis of Phase Change Problems Including Natural Convection, *ASME J. Heat Transfer*, vol. 112, pp. 812–816, 1990.
20. S. V. Patankar, *Numerical Heat Transfer and Fluid Flow*, McGraw-Hill, New York, 1980.